

Exploiting Textile Mechanical Anisotropy for Fabric-Based Pneumatic Actuators

Leonardo Cappello,^{1,2} Kevin C. Galloway,^{1,2} Siddharth Sanan,^{1,2} Diana A. Wagner,^{1,2} Rachael Granberry,^{1,2} Sven Engelhardt,^{1,2} Florian L. Haufe,^{1,2} Jeffrey D. Peisner,^{1,2} and Conor J. Walsh^{1,2}

Abstract

Knit, woven, and nonwoven fabrics offer a diverse range of stretch and strain limiting mechanical properties that can be leveraged to produce tailored, whole-body deformation mechanics of soft robotic systems. This work presents new insights and methods for combining heterogeneous fabric material layers to create soft fabric-based actuators. This work demonstrates that a range of multi-degree-of-freedom motions can be generated by varying fabrics and their layered arrangements when a thin airtight bladder is inserted between them and inflated. Specifically, we present bending and straightening fabric-based actuators that are simple to manufacture, lightweight, require low operating pressures, display a high torque-to-weight ratio, and occupy a low volume in their unpressurized state. Their utility is demonstrated through their integration into a glove that actively assists hand opening and closing.

Keywords: fabric-based actuators, mechanical programming, textile layers, soft robotic glove

Objective

SOFT ACTUATORS PRODUCE motion by deforming inherently compliant structures (e.g., elastomers) through power sources, such as compressed fluids,^{1–10} shape memory alloys,^{11–13} cables,^{14–16} voltage potential drop,¹⁷ combustion,¹⁸ catalytic decomposition,¹⁹ and various combination of these methods.²⁰ A common feature of many of these approaches is the reliance on elastomeric materials, such as silicon and urethane, for the actuator body. These materials offer many advantages, including heat and chemical resistance, the ability to co-mold multiple materials, and the ability to survive large deformations while performing complex ranges of motion.

While properties such as material density, stiffness, and strength make elastomeric materials ideal for many applications, elastomer-based actuators designed for on-body applications can restrict range of motion due to stiffness and material weight. In addition, the relationship between weight and strength can limit size scaling of soft actuator designs. Inflatable soft actuators^{2–10,21,22} are commonly constructed from elastomeric materials either as monolithic or layered structures with embedded chambers. By encoding anisotropic

properties into the body of these structures through geometry and material choice, elastomeric structures can expand in regions that are less stiff to produce a nearly infinite combination of motions.^{4–6,8,21–24}

However, these capabilities are not unique to elastomeric materials. Textiles also offer a wide range of stretch and strain properties that, when strategically utilized, can produce comparably complex motions desired in the design of soft actuators.

In this article, we aim to provide a detailed record of how three-dimensional (3D) actuators can be constructed from the two-dimensional (2D), cut-and-sew production methods commonly found in apparel manufacturing. Specifically, we show how bending and straightening motions can be supported in a single actuator by varying the arrangement of textile layers that are strained when sewn together and a thin airtight bladder is inserted between them and inflated (Fig. 1A). Moreover, we demonstrate how this fabrication method enables material combinations that produce complex, multi-degree-of-freedom actuators.

These fabric-based actuators were empirically characterized to understand how output force and torque depend on actuator pressure and what range of motion can be achieved

¹John A. Paulson School of Engineering and Applied Sciences, Harvard University, Cambridge, Massachusetts.

²Wyss Institute for Biologically Inspired Engineering, Harvard University, Cambridge, Massachusetts.

when unconstrained. In addition, we present a qualitative description of the surface mechanics of the material layers that generate bending motion to provide guiding design principles for material selection.

Finally, we demonstrate the utility of fabric-based actuators by integrating them into an assistive glove that is capable of actively opening and closing a hand while being nearly mechanically transparent to the wearer in its unpowered state.

From 2D Manufacturing to 3D Actuators

Textiles are 2D conformable materials that can be used to produce 3D structures with simple, 2D manufacturing methods. Textiles find applications in many fields, including apparel, industrial, medical, and civil engineering.²⁵ This research focuses on knit and woven textiles, schematized in Figure 1A, which are, for the purpose of this research, considered contrasting structures in terms of their mechanical compliance when load is applied on grain (i.e., in the x and y axes). A woven textile consists of vertical warp yarns interlaced with a continuous perpendicular fill, or weft yarn. Alternatively, knitted textiles are produced by interlocking loops composed of a single yarn (i.e., weft knits) or multiple yarns (warp knits).²⁶

While the strain properties of woven fabrics are primarily dependent on the strain properties of the yarns that compose them, the strain properties of knitted fabrics are dependent on both yarn and structural compliance. Consequently, a fabric-based actuator can achieve complex kinematics when knit and woven fabrics are combined and layered in such a way that differential deformations occur within the 3D structure.^{7,27,28}

The wide variety of commercially available textiles with different load-strain characteristics makes them a suitable source material for building anisotropy into the body of the actuator. Figure 1A depicts this concept where a thin-film bladder is placed between two layers of textile with different strain properties. Upon pressurization of the bladder, the top layer (i.e., high-strain knit) preferentially strains in longitudinal direction, while the bottom layer (i.e., low-strain woven) limits strain in all directions to generate the bending motion rendered in Figure 1C.

The function of the bladder is to hold air while not impeding the actuator's range of motion. It is purposefully sized larger than the textile shell such that, under pressurization, the circumferential and longitudinal stresses carried by the bladder material are negligible compared to the textile.

Furthermore, textiles enable the introduction of other geometric features such as gathers, folds, darts, or pleats, as explored in this study, which can augment the fabric's overall anisotropic behavior during pressurization.

Combining Textile Layers

A fabric-based actuator's motion is defined by the contrast of textiles, specifically their material properties, used to construct them. While it is possible to develop custom ma-

terials with specific stretch and strain-limiting properties, there are uncountable off-the-shelf knit and woven materials that exhibit desirable stretch and strain-limiting mechanics.

The material chosen for the bottom layer of the fabric-based actuator, defined as strain limiting layer, has minimal strain under load. Woven textiles are highly suitable for this layer because their structures enable minimal mechanical compliance. Parachutes, seat belts, and air bags are technical applications that utilize wovens for their bidirectional stiffness.

We chose a plain weave polyamide textile (Nylon Pack Cloth; Trident) for its high elastic modulus, low weight, drapability, and sewability properties.²⁵ We experimentally determined the load-strain characteristics of specimens of the selected woven textile and report the results in Figure 1B (warp and weft directions) and Supplementary Figure S1 (Supplementary Data are available online at www.liebertpub.com/soro) (bias directions), as well as Supplementary Table S1. The elongation-until-failure in the warp direction was 76.8% at 2009.4 N and 72.2% at 1533.6 N in the weft direction. Lower elastic moduli were observed along directions not aligned with the warp and weft, as reported in Supplementary Figure S1, due to the off-grain mechanical compliance of woven structures.

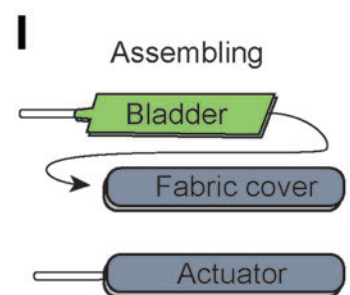
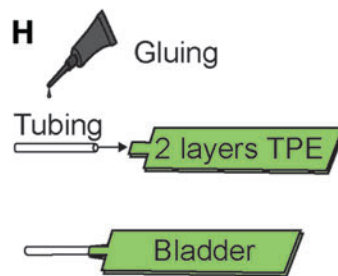
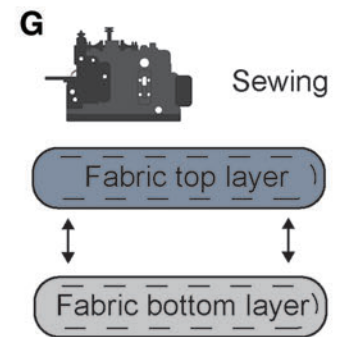
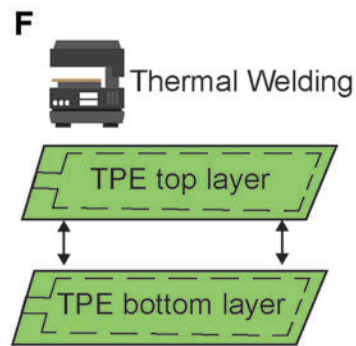
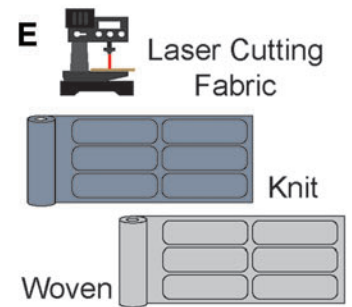
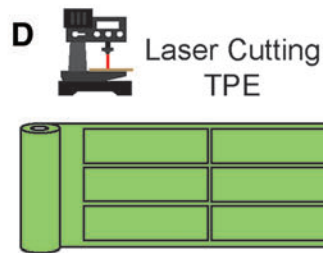
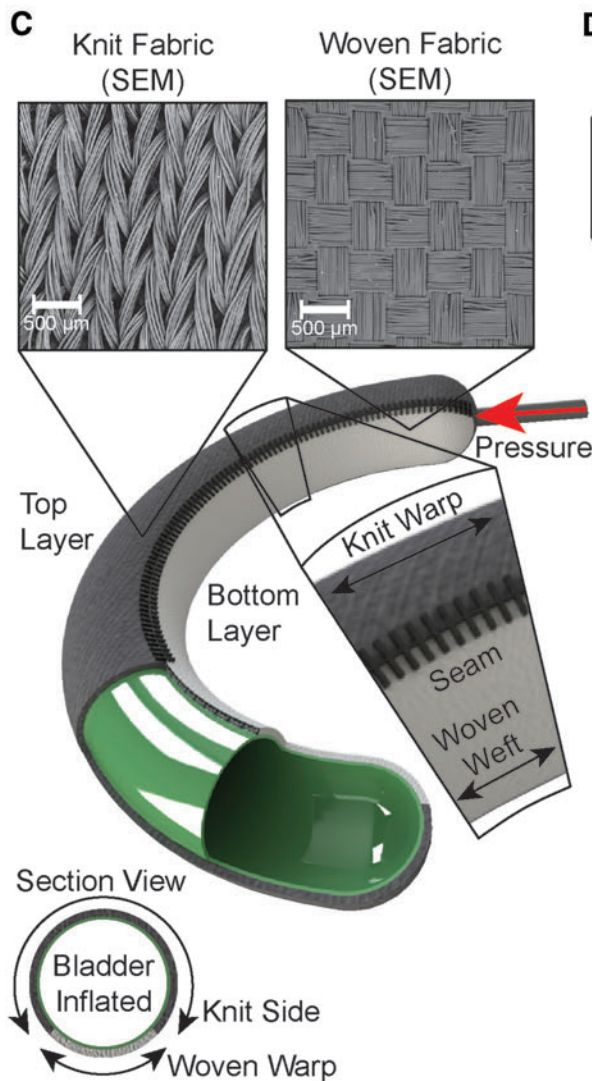
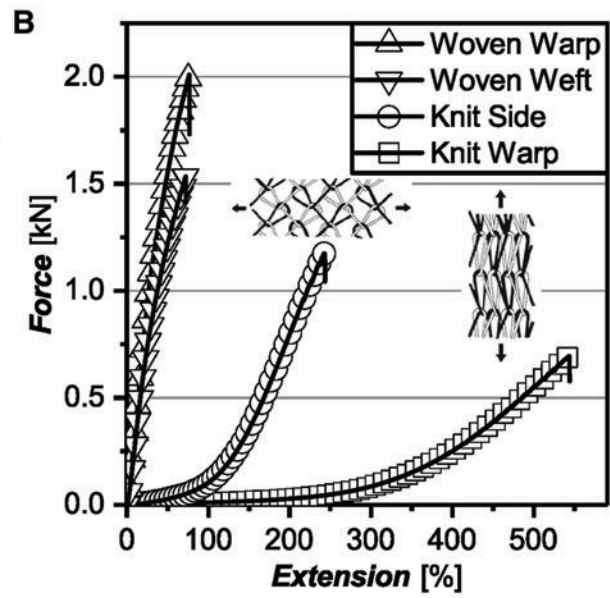
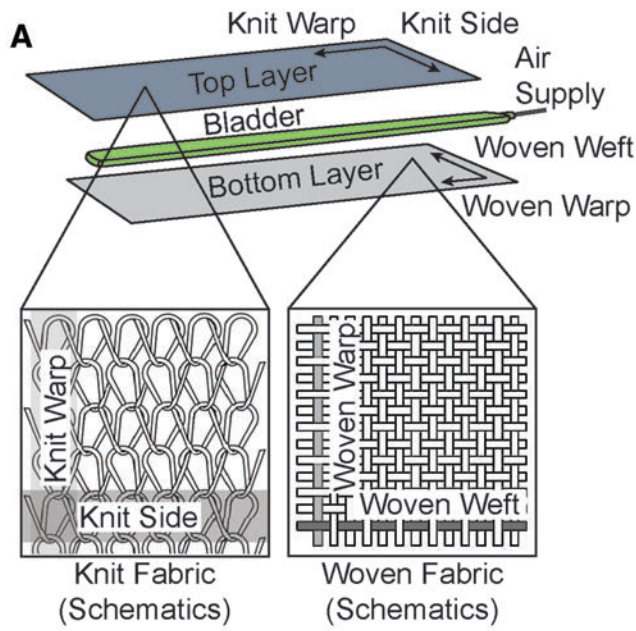
For the top layer, we desire a textile with preferential strain along a certain direction, in this case longitudinally, but with limited lateral stretch. We chose a commercially available warp-knitted raschel polyamide-elastane textile (24710; Darlington), rendered in Figure 1A, for its unidirectional stretch, durability, and stability.²⁵

Knitted materials can exhibit more pronounced anisotropic behavior than their woven counterparts because their looped construction creates inherent structural deformation biases that can be exploited along with the choice of yarn type.²⁵ Warp knits are particularly suited for applications that desire anisotropy because their structures are relatively stiff in one direction and compliant in the other. In addition, warp knits are generally balanced knits, meaning their loop structures are characterized by front-back symmetry.²⁹ While some weft knits are balanced structures (e.g., garter stitch and rib stitch), other weft knits produce asymmetrical bending (e.g., stockinette stitch). Asymmetry can result in edge curling of the fabrics, which is challenging for small scale manufacturing of our actuators and makes balanced knit structures preferable for this application.³⁰

We experimentally tested load-strain characteristics of the chosen textiles accordingly to ASTM D5034-09 standard: we cut 76 by 152 mm specimens and proceeded to test them with a universal testing machine (5566; Instron), determining the breaking strength and elongation at a constant rate of elongation of $300 \text{ mm} \cdot \text{min}^{-1}$.

The results of load-strain test on the selected knit textiles are reported in Figure 1B: the elongation until failure in warp direction was 543.3% at 694.6 N and 242.4% at 1174.8 N in side direction. The woven textile can be considered relatively inextensible compared to the knit. Scanning electron

FIG. 1. Exploiting textile mechanical anisotropy for fabric-based actuators. (A) Construction principle of fabric-based actuator capable of bending when pressurized: the top layer is made of knit textile and the bottom layer of woven textile. (B) Load-strain characteristics of woven and knit textile materials ($N=3$). (C) Operating principle: the knit textile elongates more than the woven when the bladder is inflated. (D–I) Construction steps to manufacture fabric-based actuators. Color images available online at www.liebertpub.com/soro



microscope (SEM) images of the selected textiles are depicted in Figure 1C and in more detail in Supplementary Figure S2, where the different arrangements of the yarns composing the textiles are observable.

Manufacturing fabric-based actuators

The fabric-based actuators were constructed in a multistep process. The textile actuator shell was fabricated by laser cutting (Versalaser VLS 2.30; Universal Laser Systems) the knit and woven material layers (20 × 180 mm) (Fig. 1G) and sewing them together along three edges (Fig. 1H) using a flat overlock sewing machine (MB-4DFO ActiveSeam; Merrow Sewing Machine) to form a sleeve. A short edge was left open to allow for subsequent insertion of the bladder. The overlock machine was chosen because the stitches allow for large deformation (>200%) along the sewn direction and fold open to encapsulate the seam material, which decreases actuator bulk.³¹

The bladder was fabricated by first laser-cutting rectangle shapes out of thermoplastic elastomer (TPE) (Stretchlon 200; Fiber Glast) film, 0.038 mm of thickness, (Fig. 1D) with dimensions of 30 mm in width and 200 mm in length. Subsequently, two identical layers of TPE were thermally welded along three edges with an impulse sealer (100182; American International Electric) (Fig. 1E) and finally a polyurethane tube (5790K15; McMaster-Carr) with outer diameter of 3.175 mm was glued (1360694; Loctite) to the open edge of the bladder (Fig. 1F). The bladder was inserted into the textile shell (Fig. 1I), and the open edge of the textile sleeve was hand sewn to avoid any possible puncture of the bladder.

Augmenting material layer anisotropy through pleats

While flat material layers can be combined to build functional actuators, maximizing the anisotropy of the top layer can increase the actuator's range of motion and output force. We explored this concept with an added process step that consists of pleating the textile. Pleating allows for additional material to be folded to create a hierarchical structure that further increases the anisotropy of the textile layer. Pleating is commonly used in the construction of inextensible structures where extension is required (e.g., elbow and knee joints of space suits). Consequently, larger deformation along a given direction is produced, as highlighted by the results of the load-strain tests that we performed on pleated specimens, reported in Figure 2A (83.1 N at 500% elongation, see Supplementary Table S2 for details).

To perform the load-strain characterization, pleated layers were stabilized with overlock seams on the sides. The altered motion of the pleated fabric-based actuator results from unfolding the additional material of the pleats (schematized in Fig. 2B). Figure 2C and D portray two versions, respectively, named nonpleated and pleated actuators, constructed using the aforementioned manufacturing procedure with one additional step being the pleating of the textile before laser

cutting. Pleats with ratio 3:1 (defined as the ratio between the length of the textile before and after pleating) (Fig. 2B) are obtained by folding the textile along the warp direction of the knit; the seams on the sides connecting the top with the bottom layer have the extra function to stabilize the pleats and prevent them from unintentional unfolding.

Comparison between nonpleated and pleated fabric-based actuators

The pleated and nonpleated approaches exhibit similar bending behavior; however, the pleated configuration achieved a tighter curvature, as shown in Figure 2C and D.

We characterized the variation of curvature of each fabric-based actuator with respect to pressure by inflating each specimen up to 172.4 kPa (25 psi) with linear increment of 17.2 kPa · s⁻¹ using a pressure regulator (ITV1031; SMC). Pressure was measured using a digital gauge (ASD-XAVX100PGAA5; Honeywell), and a video stream of the fabric-based actuator was recorded at 10 fps using a USB-webcam (HD C615; Logitech). An automated method based on edge detection and circle fitting algorithms (Supplementary Fig. S3) running in a real-time environment (Simulink Real-Time; MathWorks) was used to determine curvature.^{32,33} The actuator pressure signal was synchronously acquired with a data acquisition (DAQ) board (PCIe-6259; National Instruments).

Results reported in Figure 2E show that the nonpleated approach reached a curvature of 52.0 m⁻¹ while the pleated configuration reached curvature of 98.9 m⁻¹ under the same maximum pressure of 172.4 kPa (25 psi).

A custom torque rig (Supplementary Fig. S4) was built to measure the torque exerted by the fabric-based actuator when constrained to a prespecified bending angle using a hollow cylinder. The torque was measured using a force/torque sensor (Gamma; ATI Industrial Automation) that was connected to the cylinder. A clockwise torque in the plane of the rig is registered as a positive torque.

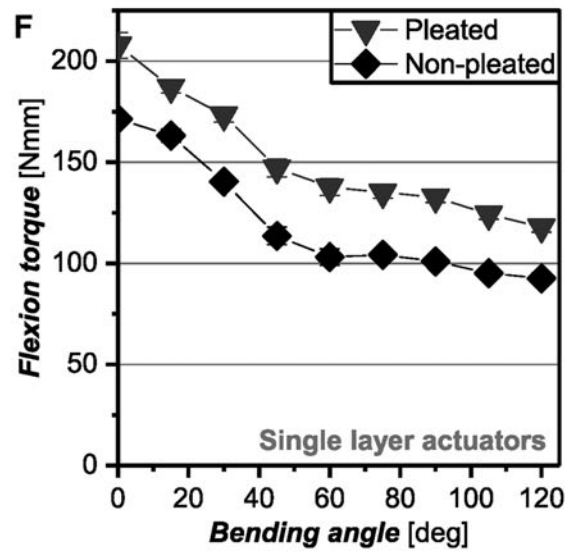
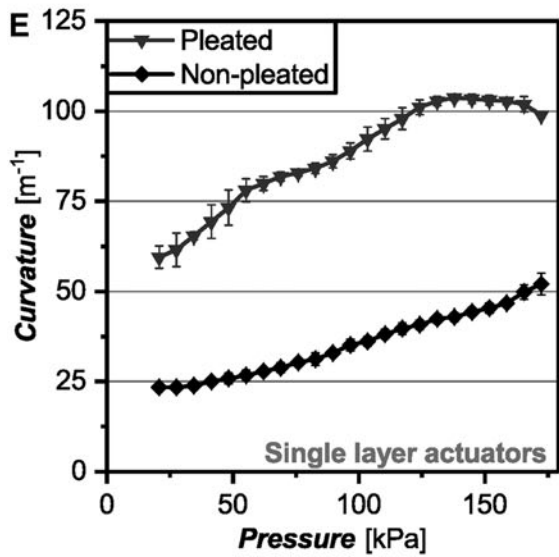
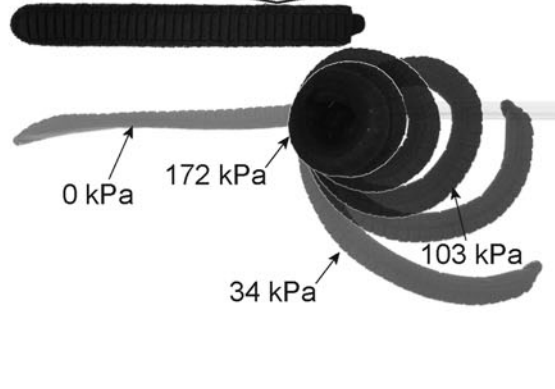
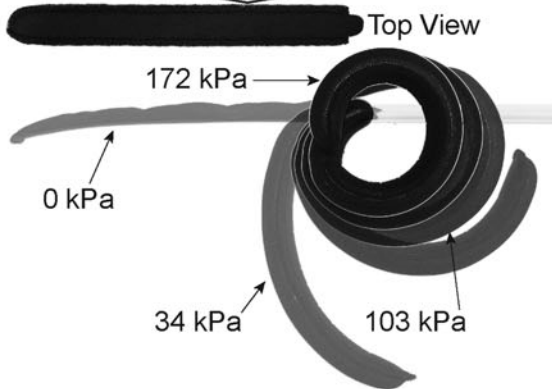
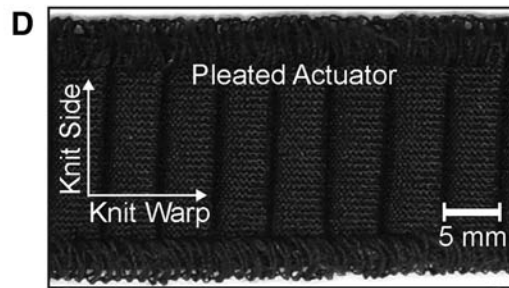
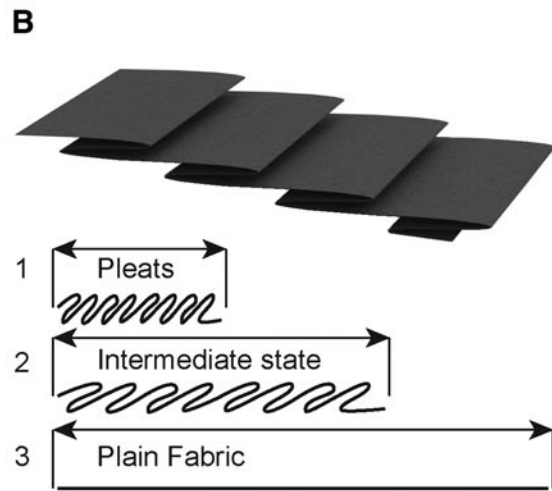
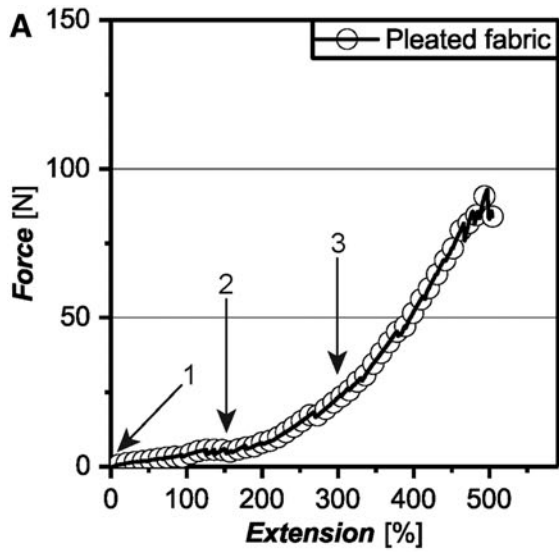
The results reported in Figure 2F indicate that the pleated approach generated more torque, with a measured maximum of 207.8 N · mm at 0° of bending when pressurized at 172.4 kPa (25 psi). In comparison, the nonpleated approach generated 171.4 N · mm under the same bending and pressure conditions.

Because the nonpleated and pleated approaches both use identical fabric materials in their construction, the larger free curvature (i.e., the curvature when not in contact with any object that would constrain its movement) and torque achieved at any given pressure with the pleated approach relative to the nonpleated one can be attributed entirely to the folds in the textile.

Achieving bidirectional motion

A significant advantage of the multilayered and multi-material fabric-based actuators is the ease with which additional degrees of freedom can be added by creating additional

FIG. 2. Nonpleated and pleated fabric-based actuators. (A) Load-strain characteristics of pleated knit textile (N=3). (B) Schematic representation of pleats. (C) Nonpleated approach and stills of pressurized states. (D) Pleated approach and stills of pressurized states. (E) Curvature of nonpleated and pleated fabric-based actuators at different pressures (N=5). (F) Output torque of nonpleated and pleated fabric-based actuators at different bending angles (N=5).



pockets. For example, the plain-woven polyamide textile (Nylon Pack Cloth; Trident) was used to create a second pocket by adding an additional bottom layer. The resulting fabric-based actuator then comprises two chambers that share a middle layer, as illustrated in Figure 3A, with two identical bladders inserted in each.

When pressurized, the new second pocket approximates a rigid beam because there is no strain property contrast between the two layers. Conveniently, it retains the ability to bend when unpressurized, which allows the full structure to bend when the alternative chamber is pressurized. Likewise, since the elastic modulus of the knit textile is significantly lower compared with the woven, the knit layer has minimal influence on the behavior of the straightening chamber. Given the flexibility of the textile, the additional woven layer and TPE bladder minimally impede the range of motion of the fabric-based actuator, as can be observed by comparing Figures 2C and 3C. Given this result, we assume that the straightening chamber does not noticeably degrade performance in terms of measured output torque and achievable curvature.

To validate our assumption, we produced two actuators with straightening chambers in pleated and nonpleated configurations (Fig. 3C, E), and we repeated the experimental test to record the bending-torque characteristics. Figure 3D and F reports the torque measured at different angular values when the fabric-based actuators were pressurized at 172.4 kPa (25 psi). Maximum torque values of 135.1 and 153.3 N·mm generated by the straightening chambers, respectively, for nonpleated and pleated approach, have been recorded at 120°.

Results confirm that the extra layer of woven textile has minimal impact on bending performance (Supplementary Fig. S5) and that the bottom chamber produces restoration torque to recover the straight configuration. Moreover, we can observe that the construction type of the bending chamber, that is, nonpleated or pleated, does not significantly affect the straightening chamber. The torque that the fabric-based actuator generates decreases as it is bent close to the free curvature at a given pressure, as described in the next section. We expected that at 0° the straightening chamber generates no torque, while the bending chamber generates maximum torque. Experimental results (Fig. 3D, F) supported this assumption.

Compared to our previous work on fiber-reinforced soft actuators,³⁴ the proposed fabric-based actuators feature the following advantages: ease of integrating textiles with different properties (e.g., strength, abrasion resistance, conductance, and so on), textile-like flexibility when unpressurized, stiff actuated states when pressurized, lower weight (4.2 g—85.3% less), lower operating pressure (172.4 kPa—58.2% less), higher torque-to-weight ratio (49.5 N·[m·kg⁻¹—95.2% more), lower volume in unpressurized state (5400 mm³—77.1% less), scalability, and custom geometries. Finally, compared to elastomeric actuators, fabric-based actuators will be less stiff when uninflated due to the inherent drapability of fabrics.

The active bidirectional motion (bending and straightening) generated by these fabric-based actuators represents an improvement with respect to the previous design of elastomeric actuators,^{5,8,24,34} where straightening motion was obtained by exploiting passive elastic forces of the actuators' bodies. For this reason, concerns related to hysteretic be-

haviors that are inherent with elastomeric actuators are mitigated in pneumatic fabric designs. In fact, the two pneumatic lines within the fabric pockets can be independently controlled. Simultaneous inflation of the two bladders with different pressurization patterns will allow fine-tuned forces and movements.

Qualitative Description of Surface Mechanics

In this section, we present a qualitative description of the surface mechanics of the material layers that generate the characteristic bending motion of the fabric-based actuators. More specifically, simplified models are presented that are intended to provide design principles for material selection. For this purpose, it is assumed that the textile thickness is negligible relative to the overall size of the actuator. Under this assumption, their motion can be inferred by understanding the motion of the 2D surface of the fabric-based actuator.

The Pneumatic Artificial Muscle (PAM, e.g., Fluidic Muscle; Festo GmbH) schematized in Figure 4A serves as an illustrative example. Its braided surface can be cut across a line parallel to the longitudinal axis (red line in Fig. 4A) and then folded flat. The flattened braided surface behaves like a tessellation of scissor mechanisms that can expand along its width while simultaneously contracting along its length. This motion corresponds to the longitudinal contraction and radial expansion of the PAM. In the absence of the braided shell, the motion of the PAM is governed solely by the mechanics of the bladder material. In the following paragraphs, we will derive the surface motion that is needed for bending fabric-based actuators.

The bending fabric-based actuators presented in this article utilize textiles with anisotropic behavior under tension, where the anisotropy is designed to result in bending motion of the system. Similar concepts have been explored with elastomeric actuators reinforced with geometry and/or fibers that result in extension, bending, twisting, and a combination of such motions.^{1,4,28} The use of textiles allows a lightweight construction owing to the relatively low thickness of the textiles (usually <1 mm) while at the same time offering significant strength in tension (>1000 N·m⁻¹).

To derive the surface motion of a bending fabric-based actuator, we will assume that its reference configuration is a cylinder and its cross section remains circular. Bending motion corresponds to a transformation of the cylinder into a torus (Fig. 4B). Note that in Figure 4B, the single red line in the 3D fabric-based actuator geometry corresponds to the two red directed edges on the surface patch. Let Equation (1):

$$f(u, v) = (f_1(u, v), f_2(u, v))^T \quad (1)$$

describe the deformation that maps a point (u, v) on the surface of the straight cylinder to the point (p, q) on the surface of the torus. The deformation $f(u, v)$ is given by:

$$\begin{pmatrix} p \\ q \end{pmatrix} = \begin{pmatrix} u + (a - a \cos(\frac{v}{a})) \frac{u}{b-a} \\ v \end{pmatrix} \quad (2)$$

where a is the radius of the cylinder, and b is the radius of curvature of the fabric-based actuator.

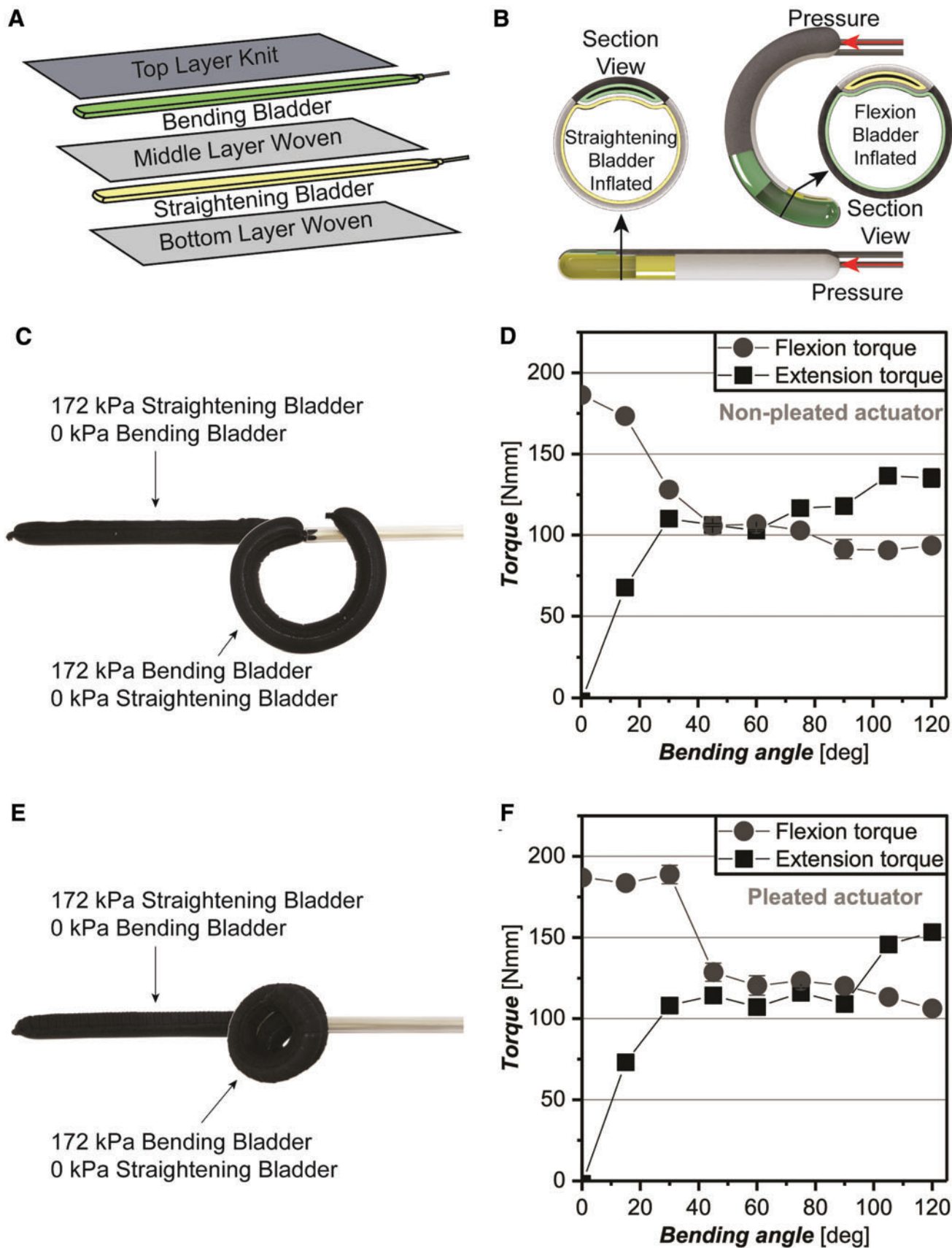


FIG. 3. Bidirectional fabric-based actuator. **(A)** Construction approach. **(B)** Operating principle: straightening and bending motion is obtained when the respective chambers are pressurized. **(C)** Stills of a bidirectional nonpleated fabric-based actuator when straightening and bending bladder is pressurized. **(D)** Output torque for the bending and straightening direction of nonpleated fabric-based actuator ($N=5$). **(E)** Stills of a bidirectional pleated fabric-based actuator when straightening and bending bladder is pressurized. **(F)** Output torque for the bending and straightening direction of pleated fabric-based actuator ($N=5$). Color images available online at www.liebertpub.com/soro

By studying the properties of Equation (2), we can gain insight into the motion characteristic of the surface. Consider the path along the cylinder with boundary defined by $u=0$ and $u=1$ (Fig. 4B). The net deformation due to $f(u, v)$ of this surface patch of unit width is given by:

$$\begin{pmatrix} \delta u \\ \delta v \end{pmatrix} = \begin{pmatrix} (a - a \cos(\frac{v}{a})) \frac{1}{b-a} \\ 0 \end{pmatrix}. \quad (3)$$

The deformation of the patch described by Equation (3) is shown graphically in Figure 4B for $a=1$ and $b=3$. From Figure 4, it is clear that the material needs to strain the most at $v=\pi$ and requires no strain at $v=0$ ($v=2\pi$ corresponds to $v=0$).

If a textile-like material or thin sheet is programmed to preferentially deform according to Equation (3) then we can achieve bending of the fabric-based actuators based on the geometric characteristics of the motion alone.

The assumption of a circular cross section is physically realistic for the same reason that a thin air or water tube (e.g., a tire tube) assumes a circular cross section when pressurized. However, a fabric-based actuator with a rectangular cross section can be used to develop a simple and intuitive understanding of the surface motion needed for a bending actuator. As can be seen from Figure 4C, the fabric-based actuator transforms from a straight tube to a segment of a bent tube with a rectangular cross section upon pressurization. This bending motion corresponds to a longitudinal elongation of the top layer, while the bottom surface does not undergo any transformation. Therefore, an approximation consisting of a top surface that preferentially elongates in the longitudinal direction and a bottom layer that is inextensible will be kinematically consistent with the motion of a bending fabric-based actuator.

Pressure-curvature and curvature-torque model

Assuming a maximum strain ratio η for the top layer, an approximation for the maximum achievable bend angle θ_{\max} for an actuator of length of l and width w can be made as:

$$\theta_{\max} = \eta \frac{\pi l}{2w} \quad (4)$$

Normalizing Equation (4) by the length l provides an expression for the maximum curvature κ_{\max} :

$$\kappa_{\max} = \eta \frac{\pi}{2w} \quad (5)$$

From Equations (4) and (5), a material with a larger strain ratio in the longitudinal direction will allow larger curvatures and bend angles for the fabric-based actuators. Along the width (circumferential direction) high strength reinforcement fibers will allow higher pressures since these fibers constrain

the cross section of the actuator and support pressure loads in the hoop direction. Since the actuators bend in approximately circular shape, a constant radius of curvature is assumed, the actuator configuration can also be described by the curvature of Equation (6):

$$\kappa = \frac{\theta}{l} \quad (6)$$

We shall refer to the bend angle and curvature assumed by the fabric-based actuators when not in contact with environment as the free bend angle θ_{free} and free curvature κ_{free} .

As previously shown, the bending fabric-based actuator assumes a finite curvature κ_{free} at any given pressure $p > 0$. From the large-deflection extension of Euler-Bernoulli beam theory,³⁵ we know that the torque τ applied on a straight cantilevered beam is proportional to the curvature of the beam described in Equation (7):

$$\tau = EI\kappa, \quad (7)$$

where E is the Young's modulus of the material, and I is the second moment of area of the beam. A similar extension can be made for precurved beams that naturally assume a free curvature κ_{free} in the absence of external loads. For such precurved beams, the torque required to drive the beam to an arbitrary curvature κ can be given by Equation (8):

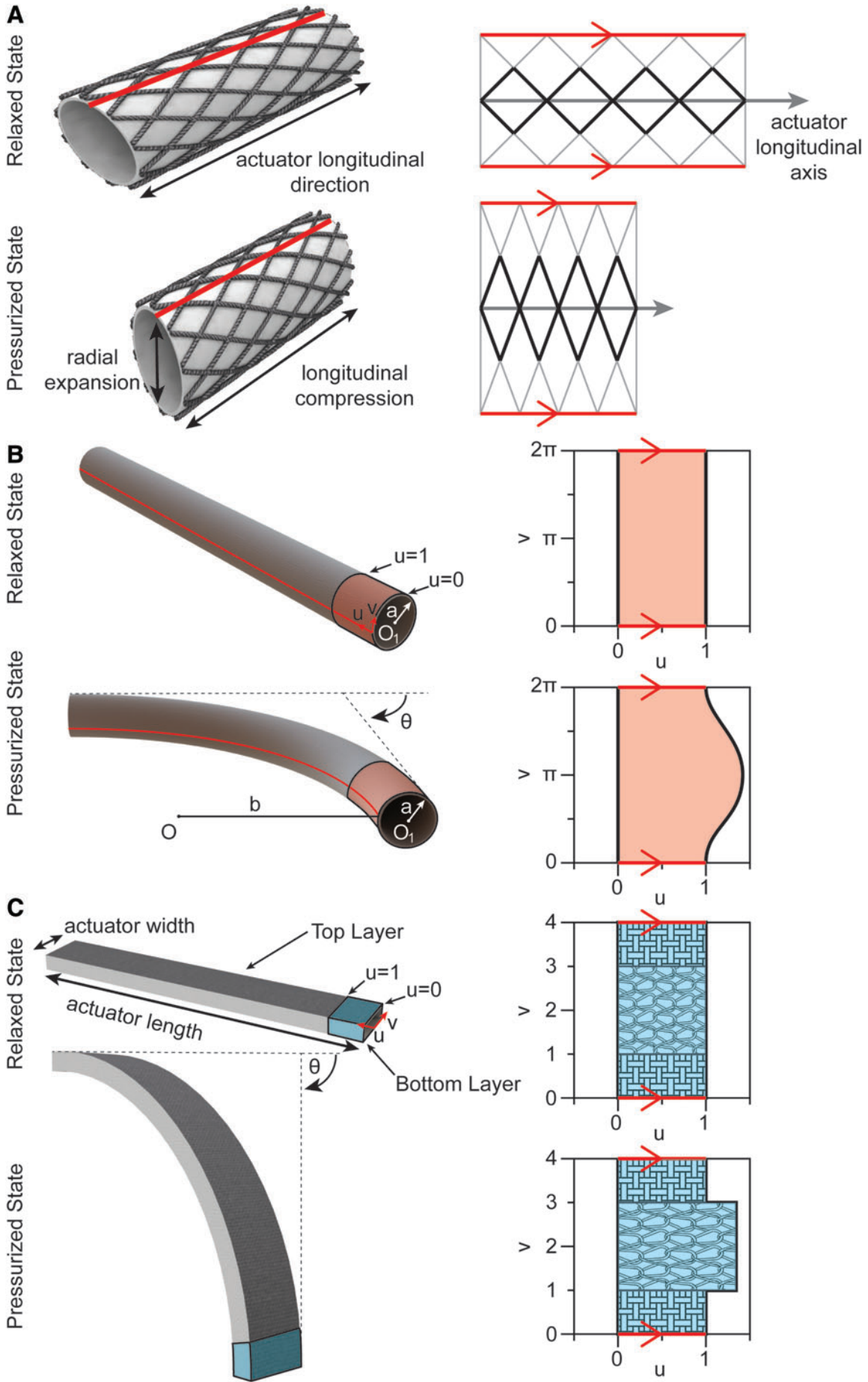
$$\tau = EI(\kappa - \kappa_{\text{free}}). \quad (8)$$

For torque characterization, we consider the bending fabric-based actuator as precurved beams with a free curvature $\kappa(p)_{\text{free}}$ that is a function of its internal pressure. The additional material folded into the pleats increases the effective maximum strain ratio for the top layer textile. For instance, if l is the length of the textile, n is the number of pleats, $l_p > 0$ is the length of the material folded in each pleat, and the maximum strain ratio is η , then the effective maximum strain ratio η_{eff} for the pleated material is given by:

$$\eta_{\text{eff}} = \frac{\eta l + n l_p}{l} = \eta + n \frac{l_p}{l} \quad (9)$$

The factor $n l_p / l$ in Equation (9) is the additional strain available due to pleating. It should be noted that there is no strain energy associated with this elongation (ignoring effects like energy required to unfold a pleat, etc.). We will refer to this factor as the pleated strain η_{pleat} . The load-strain graph in Figure 2A for the pleated textile has the expected characteristics of being less stiff along the length than the plain textile. Comparison of the load-strain relationship of the pleated and nonpleated material, shown in Figures 1B and 2A, confirms that the pleated material is less stiff than the nonpleated material along the length (strain direction).

FIG. 4. Qualitative description of surface mechanics. (A) Operating principle of Pneumatic Artificial Muscles (McKibben Actuators). (B) Surface deformation of a bending fabric-based actuator with circular cross section and normalized circumference of 2π . (C) Surface deformation of a bending fabric-based actuator with *rectangular* (approximated) cross section, negligible thickness, and normalized width of 2. In this approximation the bottom layer (represented as a woven textile) does not stretch, while the top layer (represented as a knit textile) stretches to obtain bending. Color images available online at www.liebertpub.com/soro



Equation (9) can be used to specify the total folded material nl_f that is needed for a desired η_{eff} which affects the maximum bend angle of the fabric-based actuator.

For a fabric-based actuator of length l , width w , and a top layer with effective maximum strain η_{eff} , the maximum bend angle and curvature can be obtained by substituting η_{eff} instead of in Equations (4) and (5):

$$\theta_{\text{max}} = \eta_{\text{eff}} \frac{\pi l}{2\omega} \quad (10)$$

$$\kappa_{\text{max}} = \eta_{\text{eff}} \frac{\pi}{2\omega}. \quad (11)$$

Demonstration of Fabric-Based Actuators in a Wearable Application

To demonstrate the potential of the proposed fabric-based actuators, we integrated them into a glove (Fig. 5A and Supplementary Video S1) to assist with finger flexion and extension (Fig. 5B). With its greater range of motion (i.e., larger curvature) and torque output, the pleated actuator was selected, as its performance values are closer to values obtained from the human hand.^{36,37}

To evaluate the grasp force exerted by the proposed device, we instructed a healthy participant to wear the glove and allow it to move the hand toward a gripping motion around an instrumented cylinder upon pressurization while remaining as passive as possible. In particular, we used an acrylic cylindrical tube with a diameter of 76 mm wrapped with an ultrathin pressure mapping sheet (5250; TekScan, Inc.) to measure the contact pressure. In addition, we recorded the activity of the Flexor Digitorum Superficialis (FDS) muscle using a wireless surface electromyographic (EMG) system (Trigno Lab; Delsys) with sampling frequency of 1500 Hz, rectified and filtered with a fourth order Butterworth filter with cutoff frequency of 10 Hz. The subject gave informed consent, and testing was approved by the Harvard Medical School Institutional Review Board (IRB).

A peak contact pressure of 13.0 kPa and an overall contact force of 15 N were recorded when the bending chambers were inflated with a pressure of 172.4 kPa (25 psi) (Fig. 5C). Assuming a coefficient of static friction of 0.5, the results indicate that the grip force generated by the glove is sufficient to grasp objects up to a weight of 750 g, representing the majority of the objects encountered during activities of daily living.³⁸ During the experiment, EMG activity of the flexor muscles of the fingers was found to be 4.3% of the maximum voluntary contraction (MVC) and not distinguishable from the baseline EMG activity, indicating that the participant did not actively contribute to the grasp force.

A further experimental trial was conducted to evaluate the assistive action of the glove. The participant was instructed to: (1) relax their hand muscles, (2) actively close their hand, (3) relax their hand muscles again, and (4) actively open their

hand without the assistive glove. Subsequently, the participant donned the assistive glove and was instructed to allow the glove to close and open their hand. The activity of the FDS and Extensor Digitorum Communis (EDC) muscles of the participant was recorded during the whole trial. This procedure was repeated thrice, after which the EMG activity during MVC was acquired.

The EMG activity associated with the execution of the movements decreased by 65.9% (from 15.5% to 5.3% of MVC) during hand closing and by 76.7% (from 27.4% to 6.4% of MVC) during hand opening to values indistinguishable from baseline activity (Fig. 5D).

Conclusion

In this study, we presented methods to exploit the mechanical anisotropy of knit and woven textiles to create fabric-based actuators that can achieve motions suitable for wearable applications.

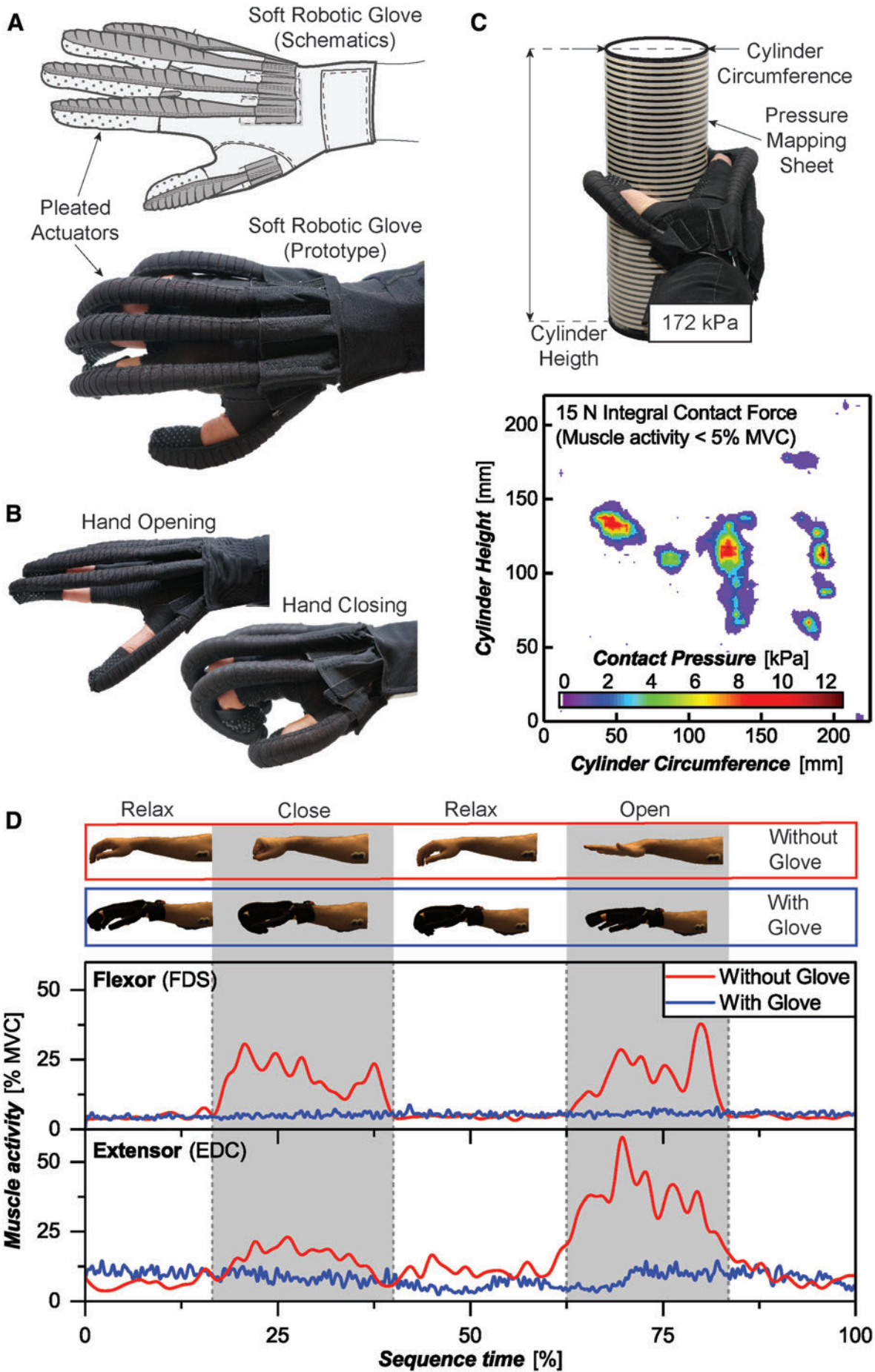
We demonstrated that manufacturing methods for 2D materials can be leveraged to combine textile layers with different stretch and strain-limiting properties to create a variety of 3D motions. Furthermore, by introducing geometrical variations into the structure, that is, pleats, it is possible to increase the anisotropy of the textiles and ultimately to increase the range of motion and force output of an actuator with the same pressure input as the nonpleated actuator. We implemented fabric-based actuators able to both bend and straighten to demonstrate that complex motions can be achieved by simply layering different, commercially available textiles, specifically, a knit textile as the top layer, combined with two layers of plain woven textiles.

We also proposed a qualitative description of the surface mechanics governing the multilayer construction of the fabric-based actuators presented in this study. However, this method is far from exhaustive, and further research and modeling work are needed to fully describe the proposed actuators. The main challenge of this theoretical approach is finding constitutive models that accurately describe the complex behavior of textiles under loading. Textiles have a complex microstructure that makes it difficult to predict stretch deformation, and anisotropy further complicates this modeling work. Moreover, developing an analytical model of the overall deformation of fabric-based actuators represents another open challenge that future research must tackle due to their nonlinear behavior when pressurized.

The data gathered in this work represent the first of the many steps necessary to analytically characterize fabric-based actuators.

By integrating these fabric-based actuators into a glove, we demonstrated that they can generate assistive grasping force during activities of daily living. This approach highlights the potential of fabric-based actuators, as the proposed device can assist hand movements when pressurized and remain lightweight. The weight of the assistive glove is, 78.6 g, comparable to the weight of a standard padded wheelchair

FIG. 5. Glove constructed using fabric-based actuators. (A) Schematic of a glove. (B) Achievable motions with the proposed device. (C) Pressure mapping of the glove while grasping an instrumented cylinder. (D) Muscle activity of a healthy subject during an experimental trial without the glove and with the powered glove. Color images available online at www.liebertpub.com/soro



glove, which weighs 60.5 g (PWC200; Hatch Gloves). Clinical research studies are currently being conducted by our group to demonstrate that the glove presented in this article can effectively assist the capability of impaired users to grasp and manipulate objects of daily living.³⁹

We envision expanding the functionality of our fabric-based actuators by adding sensing capabilities through fabric-based sensors⁴⁰ to capture movement and interaction data. Future research will also investigate pressurization patterns and closed-loop controllers to fully demonstrate the potential of these actuators. More actuation modes (e.g., creating multiple joints within the same actuator) will also be added to achieve motions conformable to the body, which is possible with simple 2D manufacturing methods (e.g., alternating textiles with different strain properties in the top layer).

Acknowledgments

This work was supported by the National Science Foundation (Grant Nos. 1454472 and 1317744), the Wyss Institute for Biologically Inspired Engineering, and the Harvard John A. Paulson School of Engineering and Applied Sciences. The authors thank Dr. James Weaver for help with SEM images and Dr. Fausto Panizzolo for the help with EMG data collection and processing.

Author Disclosure Statement

No competing financial interests exist.

References

1. Chou C-P, Hannaford B. Measurement and modeling of McKibben pneumatic artificial muscles. *Robot Autom IEEE Trans* 1996;12:90–102.
2. Suzumori K, Endo S, Kanda T, *et al.* A bending pneumatic rubber actuator realizing soft-bodied manta swimming robot. *Proc IEEE Int Conf Robot Autom* 2007; 4975–4980.
3. Noritsugu T, Takaiwa M, Sasaki D. Power assist wear driven with pneumatic rubber artificial muscles. *15th Int Conf Mechatronics Mach Vis Pract M2VIP'08* 2008;539–544.
4. Shepherd RF, Ilievski F, Choi W, *et al.* Multigait soft robot. *Proc Natl Acad Sci U S A* 2011;108:20400–20403.
5. Mosadegh B, Polygerinos P, Keplinger C, *et al.* Pneumatic networks for soft robotics that actuate rapidly. *Adv Funct Mater* 2014;24:2163–2170.
6. Sun Y, Song YS, Paik J. Characterization of silicone rubber based soft pneumatic actuators. *IEEE Int Conf Intell Robot Syst* 2013;4446–4453.
7. Roche ET, Wohlfarth R, Overvelde JTB, *et al.* A bio-inspired soft actuated material. *Adv Mater* 2014;26:1200–1206.
8. Connolly F, Walsh CJ, Bertoldi K. Automatic design of fiber-reinforced soft actuators for trajectory matching. *Proc Natl Acad Sci U S A* 2017;114:51–56.
9. Galloway KC, Becker KP, Phillips B, *et al.* Soft robotic grippers for biological sampling on deep reefs. *Soft Robot* 2016;3:23–33.
10. Elgeneidy K, Lohse N, Jackson M. Data-driven bending angle prediction of soft pneumatic actuators with embedded flex sensors. *IFAC PapersOnLine* 2016;49:513–520.
11. Trimmer B, Takesian AE, Sweet BM, *et al.* Caterpillar locomotion: A new model for soft-bodied climbing and burrowing robots. In: *Proceedings of the 7th International Symposium on Technology and the Mine Problem*, Monterey, CA, May 2–5, 2006, pp. 1–10.
12. Laschi C, Cianchetti M, Mazzolai B, *et al.* Soft robot arm inspired by the octopus. *Adv Robot* 2012;26:709–727.
13. Yuen MC, Bilodeau RA, Kramer RK. Active variable stiffness fibers for multifunctional robotic fabrics. *IEEE Robot Autom Lett* 2016;1:708–715.
14. Asbeck AT, Dyer RJ, Larusson AF, *et al.* Biologically-inspired soft exosuit. *IEEE Int Conf Rehabil Robot* 2013; 2013:6650455.
15. In BH, Kang BB, Sin M, *et al.* A wearable robot for the hand with a soft tendon routing system. *IEEE Robot Autom Mag* 2015;97–105.
16. Dinh K, Xiloyannis M, Antuvan CW, *et al.* A soft wearable arm exoskeleton based on hierarchical cascade controller for assistance modulation. *IEEE Robot Autom Lett* 2017:1–8.
17. Shintake J, Rosset S, Schubert B, *et al.* Versatile soft grippers with intrinsic electroadhesion based on multifunctional polymer actuators. *Adv Mater* 2016;28:231–238.
18. Bartlett NW, Tolley MT, Overvelde JTB, *et al.* Robot powered by combustion. *Science* 2015;349:161–165.
19. Wehner M, Truby RL, Fitzgerald DJ, *et al.* An integrated design and fabrication strategy for entirely soft, autonomous robots. *Nature* 2016;536:451–455.
20. Walker ID, Dawson DM, Flash T, *et al.* Continuum robot arms inspired by cephalopods. *Proc SPIE* 2005;5804:303.
21. Correll N, Önal ÇD, Liang H, *et al.* Soft autonomous materials using active elasticity and embedded distributed computation. *Springer Tracts Adv Robot* 2014;79:227–240.
22. Martinez RV, Fish CR, Chen X, *et al.* Elastomeric origami: Programmable paper-elastomer composites as pneumatic actuators. *Adv Funct Mater* 2012;22:1376–1384.
23. Connolly F, Polygerinos P, Walsh CJ, *et al.* mechanical programming of soft actuators by varying fiber angle. *Soft Robot* 2015;2:26–32.
24. Polygerinos P, Wang Z, Overvelde JTB, *et al.* Modeling of soft fiber-reinforced bending actuators. *IEEE Trans Robot* 2015;31:778–789.
25. Pritchard M, Sarsby RW, Anand SC. *Handbook of Technical Textiles*. Cambridge, UK: Elsevier, 2000, pp. 372–406.
26. Veit D, Gries T, Wulfhorst B. *Textile Technology: An Introduction*. Munich, Germany: Hanser Publications, 2015.
27. Baldwin HA. Realizable models of muscle function. In: *Biomechanics*, Bootzin D, Muffley HC. (Eds). *Proceedings of the First Rock Island Arsenal Biomechanics Symposium*, April 5–6, 1967, Boston, MA, Springer, 1995, pp. 139–147.
28. Daerden F, Lefeber D, Verrelst B, *et al.* Pleated pneumatic artificial muscles: Compliant robotic actuators. *Proc 2001 IEEE/RSJ Int Conf Intell Robot Syst Expand Soc Role Robot Next Millenn (Cat No01CH37180)* 4:1958–1963.
29. Ray SC. *Fundamentals and Advances in Knitting Technology*. New Delhi, India: Woodhead Publishing India Pvt. Ltd., 2012.
30. Kurbak A, Ekmen O. Basic studies for modeling complex weft knitted fabric structures part I: A geometrical model for widthwise curlings of plain knitted fabrics. *Text Res J* 2008;78:198–208.
31. Colovic G. Sewing, stitches and seams. In: *Nayak R, Padhye R, eds. Garment Manufacturing Technology*. Cambridge, UK: Elsevier, 2015, p. 247.

32. Canny J. A computational approach to edge detection. *IEEE Trans Pattern Anal Mach Intell* 1986;6:679–698.
33. Pratt V. Direct least-squares fitting of algebraic surfaces. *ACM SIGGRAPH computer graphics ACM* 1987;21:145–152.
34. Polygerinos P, Galloway KC, Sanan S, *et al.* EMG controlled soft robotic glove for assistance during activities of daily living. *IEEE Int Conf Rehabil Robot* 2015; 55–60.
35. Howell LL. *Compliant Mechanisms*. New York, NY: John Wiley & Sons, 2001.
36. Eberhart HD, Inman VT, Bresler B. The principal elements in human locomotion. In: Klopsteg PE, Wilson PD, eds. *Hum Limbs Their Substitutes*. New York, NY: McGraw-Hill, 1954, pp. 437–471.
37. Keller AD. *Studies to Determine the Functional Requirements for Hand and Arm Prosthesis*. Los Angeles, CA: Department of Engineering University of California, 1947.
38. Matheus K, Dollar AM. Benchmarking grasping and manipulation: Properties of the objects of daily living. In: *IEEE/RSJ 2010 International Conference on Intelligent Robots and Systems (IROS)*, Taipei, Taiwan, October 18–22, 2010, pp. 5020–5027.
39. Cappello L, Meyer JT, Galloway KC, *et al.* Assisting hand function after spinal cord injury with a fabric-based soft robotic glove. *J Neuroeng Rehabil* 2018;15(59). DOI: 10.1186/s12984-018-0391-x.
40. Atalay A, Sanchez V, Atalay O, *et al.* Batch fabrication of customizable silicone-textile composite capacitive strain sensors for human motion tracking. *Adv Mater Technol* 2017; 1700136:1–8.

Address correspondence to:

Conor J. Walsh

School of Engineering and Applied Science

Harvard University

29 Oxford St., Room 328

Cambridge, MA 02138

E-mail: walsh@seas.harvard.edu